THE JOURNAL OF BIOLOGICAL CHEMISTRY VOL. 286, NO. 2, pp. 1364–1373, January 14, 2011

Structural Analysis of the Conserved Ubiquitin-binding Motifs (UBMs) of the Translesion Polymerase iota in Complex with Ubiquitin*[S]

Received for publication, April 16, 2010, and in revised form, August 26, 2010 Published, JBC Papers in Press, October 6, 2010, DOI 10.1074/jbc.M110.135038

Daniel Burschowsky[‡1], Fabian Rudolf[§¶1,2], Gwénaël Rabut[§3], Torsten Herrmann[‖], Matthias Peter[§¶4], and Gerhard Wider[‡5]

From the [‡]Institute of Molecular Biology and Biophysics, ETH Zurich, 8093 Zurich, Switzerland, the [§]Institute of Biochemistry, ETH Zurich, 8093 Zurich, Switzerland, the [¶]Competence Center for Systems Physiology and Metabolic Diseases, 8093 Zurich, Switzerland, and the [‖]Université de Lyon, CNRS/ENS Lyon/UCB, Centre Européen de RMN à très hauts champs, 5 Rue de la Doua, 69100 Villeurbanne, France

Ubiquitin-binding domains (UBDs) provide specificity to the ubiquitin system, which is also involved in translesion synthesis (TLS) in eukaryotic cells. Upon DNA damage, the UBDs (UBM domains) of polymerase iota (Pol ι) interact with ubiquitinated proliferating cell nuclear antigen to regulate the interchange between processive DNA polymerases and TLS. We report a biophysical analysis and solution structures of the two conserved UBM domains located in the C-terminal tail of murine Pol ι in complex with ubiquitin. The 35-amino acid core folds into a helix-turn-helix motif, which belongs to a novel domain fold. Similar to other UBDs, UBMs bind to ubiquitin on the hydrophobic surface delineated by Leu-8, Ile-44, and Val-70, however, slightly shifted toward the C terminus. In addition, UBMs also use electrostatic interactions to stabilize binding. NMR and fluorescence spectroscopy measurements revealed that UBMs bind monoubiquitin, and Lys-63- but not Lys-48-linked chains. Importantly, these biophysical data are supported by functional studies. Indeed, yeast cells expressing ubiquitin mutants specifically defective for UBM binding are viable but sensitive to DNA damaging conditions that require TLS for repair.

Ubiquitin plays a major role in regulating diverse biological pathways by changing the function, localization, or turnover of target proteins. In most cases, ubiquitin gets attached to an ϵ-amine of a lysine side chain via an isopeptide bond (1) and serves as a molecular tag by providing an additional binding surface, which is recognized by a plethora of different ubiquitin-binding domains (UBDs)[6] from at least 16 different families (2, 3). Most UBDs use α-helical structures to bind a solvent-exposed hydrophobic patch on the β-sheet of ubiquitin, which includes Leu-8, Ile-44, and Val-70. The amino acids surrounding this hydrophobic patch are chemically diverse, thus allowing for different binding modes (2–4). Ubiquitin can be attached on target proteins either as single (monoubiquitination) or multiple single moieties (multiubiquitination), or as several ubiquitins covalently bound to each other in a chain-like fashion (polyubiquitination). These chains can be linked to the N terminus or any of the seven different lysines of ubiquitin; Lys-11 and Lys-48 are the most frequently used, whereas Lys-48 and Lys-63 are the best studied (5). How ubiquitin tags and chains are specifically recognized by the different UBDs remains an important but poorly understood question (2, 3).

Linkage-dependent spatial conformations taken by different ubiquitin chains significantly contribute to the specificity of UBD-ubiquitin interactions. Some domains exclusively bind Lys-48- (6, 7) or Lys-63-linked ubiquitin chains (8). NMR spectroscopy revealed that individual ubiquitin moieties in Lys-63-linked chains resemble beads on a string, whereas ubiquitins in Lys-48-linked chains fold onto each other (9, 10). It remains unclear why some domains show a clear preference toward either form of ubiquitin chains. Moreover, the binding preference is not conserved within domain families (3, 11–13).

The UBD-containing proteins that bind to the ubiquitinated substrate determine the elicited biological response (2, 3). For example, ubiquitin conjugation as monoubiquitin and Lys-63-linked polyubiquitin chains emerged as important determinants to ensure faithful DNA replication and genomic stability (14). In particular, ubiquitination of the proliferating cell nuclear antigen (PCNA) is thought to signal an appropriate DNA damage response and controls the switch from processive DNA replication to translesion synthesis (TLS) at

* This work was supported by grants from the Swiss National Science Foundation, Oncosuisse, INSERM (to G. R.), and the ETH Zurich (TH-42/04-2 and TH-33 07-3).

The atomic coordinates and structure factors (codes 2KWV and 2KWU) have been deposited in the Protein Data Bank, Research Collaboratory for Structural Bioinformatics, Rutgers University, New Brunswick, NJ (http://www.rcsb.org/).

[S] The on-line version of this article (available at http://www.jbc.org) contains supplemental Tables 1 and 2, Figs. 1–13, and additional references.

[1] Both authors contributed equally to this article.

[2] Present address: BSSE, ETH-Zurich, Mattenstrasse 26, 4058 Basel, Switzerland.

[3] Present address: CNRS, UMR6061, Université Rennes 1, Institute of Genetics and Development, 35043 Rennes, France.

[4] To whom correspondence may be addressed. Tel.: 41-44-63-36-586; Fax: 41-44-63-21-298; E-mail: matthias.peter@bc.biol.ethz.ch.

[5] To whom correspondence may be addressed. Tel.: 41-44-63-33-455; Fax: 41-44-63-31-484; E-mail: gsw@mol.biol.ethz.ch.

[6] The abbreviations used are: UBD, ubiquitin-binding domain; PCNA, proliferating cell nuclear antigen; TLS, translesion synthesis; Ub, ubiquitin; UBZ, ubiquitin-binding zinc finger; CHAPS, 3-[(3-cholamidopropyl)dimethylammonio]-1-propanesulfonic acid; NOESY, nuclear Overhauser and exchange spectroscopy; UPL, upper distance limit; 4NQO, 4-nitroquinoline-1-oxide.

stalled forks. A set of conserved, error-prone polymerases can bypass the lesion, which would otherwise block DNA replication. Evidence suggests that the functional integrity of specialized UBDs classified as UBM and UBZ domains is essential for the proper localization of TLS polymerases to damage-induced stalled replication foci and for cellular survival following DNA damage (15). Interestingly, UBM and UBZ domains are less dependent on Ile-44 in the classical binding patch on ubiquitin compared with other UBDs (16), raising the question whether these domains interact with ubiquitin through a distinct binding mode.

Very recently, an NMR structure of the UBM2 domain of human polymerase iota (Pol ι) fused to GB1 (17) in complex with ubiquitin has been published (Protein Data Bank codes 2KHU and 2KHW) (18). Binding affinities of ubiquitin to the wild type and mutated fusion protein were analyzed using isothermal titration calorimetry. Confirming earlier results (16) deletion of either UBM in Pol ι abolished the localization of Pol ι to replication foci in UV-irradiated MRC5 cells, as did mutations disrupting the fold of UBM2, whereas mutations disturbing the binding interface only impaired the localization of human Pol ι and yeast Rev1.

Here, we report the NMR solution structures of the two UBM domains of the murine Y-family translesion Pol ι (see domain organization in supplemental Fig. 1) in complex with ubiquitin. Despite their low sequence identity of 25%, both small UBMs fold into a similar, previously unreported helix-turn-helix motif that is independent of its binding partner ubiquitin. Our detailed structural and mutational analysis revealed that both UBM domains bind ubiquitin using the usual binding surface for UBDs. However, not the entire hydrophobic surface of ubiquitin is used, and in addition, electrostatic interactions stabilize the binding. Fluorescence spectroscopy revealed that UBM2 excludes Lys-48-linked ubiquitin chains but binds to any freely accessible ubiquitin binding surface with similar strength. We conclude that UBM domains assemble in a novel structural fold that ensures specific ubiquitin binding by a mechanism resembling allovalency, which is important for error-free DNA synthesis *in vivo*.

EXPERIMENTAL PROCEDURES

Cloning, Expression, and Purification—UBM1 and UBM2 single domain constructs were cloned into a pGEX-4T vector as a C-terminal fusion to GST; ubiquitin was encoded on pET19b. Single amino acid substitutions used for fluorescence titrations were obtained using site-directed mutagenesis. All plasmids contained an ampicillin/carbenicillin resistance gene for selection and a *lac*-inducible T7 promotor. Clones were confirmed via sequence analysis.

Unlabeled, ^{15}N- and ^{15}N,^{13}C-labeled protein was expressed in *Escherichia coli* BL21DE3Star (Invitrogen) in LB (unlabeled) or M9 minimal medium. Cells were grown at 37 °C, induced with 0.2 mM isopropyl 1-thio-β-D-galactopyranoside (final), harvested upon growth arrest, and resuspended in lysis buffer (1× PBS, 300 mM KCl, 10% glycerol, 0.5 mM EDTA, 150 μM PMSF, cOmplete inhibitor tablets (Roche)) at a ratio of 5 ml/g wet pellet. Cells were lysed by French press and cleared of insoluble parts by centrifugation at 48,000 × *g*.

The GST-fusion proteins were bound in batch mode on freshly prepared glutathione-Sepharose beads (GE Healthcare) at room temperature for 3 h. The beads were washed five times each with lysis buffer and PBS (10 times bead volume). UBM domains were cleaved off using thrombin (Amersham Biosciences) (UBM1, 10 units/ml, 25 °C for 20 h; UBM2, 5 units/ml, 15 °C for 12 h).

For ubiquitin, the bulk of the proteins were precipitated using perchloric acid at a final concentration of 3.5% and 40 °C for 10 min. After centrifugation at 48,000 × *g*, the supernatant containing ubiquitin was neutralized using saturated Tris base solution.

Buffers were exchanged to ion exchange binding buffers (UBMs, 10 mM sodium phosphate buffer, 2.7 mM KCl, 10 mM NaCl, pH 8.5; Ub, 20 mM ammonium acetate, pH 4.5) using a HiPrep 26/10 desalting column, and the proteins were bound to a Resource Q (UBMs) or Resource S (Ub) ion exchange column, of which they were eluted by a gradient of elution buffer (UBMs, 10 mM sodium phosphate buffer, 2.7 mM KCl, 2 M NaCl, pH 8.5; Ub, 250 mM ammonium acetate, pH 7.6). Rebuffering to NMR buffer (25 mM sodium phosphate buffer, 100 mM KCl, 25 mM NaCl, 2 mM CHAPS, pH 6.0) was performed using a Superdex 75 10/30 gel filtration column. Typical yields per liter medium were 2.5 and 25 mg, for unlabeled UBMs and ubiquitin, respectively, and 1.6 and 15 mg for the corresponding labeled proteins.

NMR Analysis—All NMR experiments were performed at 15 °C. For UBM1, the initial titrations with unlabeled ubiquitin as well as heteronuclear NOE experiments were performed with ^{15}N-labeled UBM1* that contained additional flanking residues, all other experiments with UBM1 (supplemental Fig. 3).

Titrations to characterize the binding interaction and for thermal denaturation were recorded as series of [^{1}H,^{15}N]- and [^{1}H,^{13}C]-HSQC spectra, respectively. For the characterization of protein-protein interactions, the isotope-labeled compound was 7-fold overtitrated with its unlabeled binding partner. Combined chemical shift changes (Δδ) were calculated using the formulas $\Delta\delta = \sqrt{\Delta\delta(^{1}H)^2 + (\frac{1}{5}\Delta\delta(^{15}N))^2}$ for ^{1}H attached to ^{15}N and $\Delta\delta = \sqrt{\Delta\delta(^{1}H)^2 + (\frac{1}{4}\Delta\delta(^{13}C))^2}$ for ^{1}H attached to ^{13}C, respectively (19).

Chemical shift changes Δδ were fitted assuming one interaction site per molecule using the formula, $\Delta\delta = \Delta\delta_{max}(((K_D + [L_0] + [P_0]) - \sqrt{(K_D + [L_0] + [P_0])^2 - (4[P_0][L_0])})/2[P_0])$, where Δδ is the chemical shift change, $\Delta\delta_{max}$ is the chemical shift change at saturation, K_D is the dissociation constant, $[L_0]$ is the total ligand (Ub) concentration, and $[P_0]$ is the total protein (UBM) concentration (20). The maximal Δδ values were reached at ~4-fold overtitration; this ratio was used for all NMR samples to saturate the NMR-observable isotope-labeled compound in the complexes of UBMs and ubiquitin with unlabeled binding partner (supplemental Fig. 2).

Sequence-specific resonance assignment of the different constructs was based on HNCA, HNCACB (supplemental Fig. 13), and HCcH-COSY as well as ^{13}C- and ^{15}N-resolved [^{1}H-

^{1}H]-NOESY experiments. Overall, >97% of all the resonances in the spectra of the UBM·ubiquitin complexes were assigned.

For the determination of the structure of the UBM·ubiquitin complexes, ^{13}C- and ^{15}N-resolved [^{1}H-^{1}H]-NOESY experiments (mixing time, 80 ms) were acquired. For the characterization of the binding interface ^{13}C-resolved [^{1}H,^{1}H-(^{12}C-edited)]-NOESY experiments (mixing time, 120 ms) were measured of ^{13}C,^{15}N-labeled UBM domains in complex with unlabeled ubiquitin and *vice versa* (21). The NOEs in these spectra were analyzed and assigned manually and added to the otherwise automated structure calculation, during which they were verified.

Structure Calculations of UBM·Ubiquitin Complex—Structure calculations of UBM-ubiquitin complexes were performed using UNIO'08 1.0.4, which combines ATNOS/CANDID (22, 23) with different molecular dynamics programs. We used the following input: a set of ^{15}N-resolved and aromatic and aliphatic ^{13}C-resolved [^{1}H-^{1}H]-NOESYs for labeled UBM overtitrated with unlabeled ubiquitin and *vice versa* (six spectra per UBM-Ub complex), a list of ambiguous and unambiguous intermolecular upper distance constraints (UPLs) all set to 5.5 Å, a combined assignment list of both binding partners and the amino acid sequence of the complex, containing a 22-dummy residue linker between UBM and ubiquitin for CYANA (24) calculations. The lists of intermolecular UPLs (136 or 99 ambiguous and 36 or 73 unambiguous UPLs for UBM1 or UBM2, respectively) were automatically evaluated during the structure calculation using a consistency check and network anchoring (23). In the final step, 97 and 96 unambiguous intermolecular UPLs were available for the complexes of UBM1 and UBM2, respectively.

Structure calculations were performed in seven cycles with 100 structures per cycle, of which the twenty with the lowest target functions were selected for the following cycle. The molecular dynamics step of the last cycle was manually repeated with CYANA using 200 starting structures and selecting the 40 best structures, which were used as input for energy minimization and refinement using AMBER9 (25) with the force field ff99 (26). The final structures are represented by the 20 complex structures with the lowest energy (Table 1; see Fig. 1, *A* and *B*, and Fig. 2, *B* and *C*). MOLMOL (27) was used to analyze the conformers and to prepare the figures showing molecular models.

Fluorescence Titrations—Increasing amounts of ubiquitin were added to the UBM2 domains, whose intrinsic tryptophan fluorescence signal was monitored. The measurements were performed at 24 °C with initial concentrations of UBM2 of 30 μM; excitation and emission wavelengths were at 280 and 345 nm, respectively. Titrations were repeated four times, and the binding curves were fitted using $F = F_A \times \bar{C}_A + \Delta F \times \frac{1}{2}(g - \sqrt{g^2 - h})$, where $g = \bar{C}_S + K_D + p\bar{C}_A$, $h = 4p\bar{C}_A\bar{C}_S$, and $\Delta F = F_{AS} - F_A$. F_A and F_{AS} represent the fluorescence signal of free protein A (UBM2) and the complex AS (UBM2·Ub), respectively, $\bar{C}_A$ is the total concentration of UBM2, $\bar{C}_S$ is the total concentration of the substrate S (Ub), and p is the stoichiometry value (28).

Yeast Strains and Yeast Assays—All yeast strains used in this study (supplemental Table 1) were derived from LHY461 (4), where the four endogenous Ub genes have been deleted, and Ub is only expressed from a LYS2-marked plasmid. Strains expressing Ub mutants were obtained by transforming LHY461 with URA3-marked plasmids encoding wild type or the T66A, H68A, and T9A Ub mutants (4). The transformants were propagated on a medium containing aminoadipate to counterselect the LYS2-marked plasmid and therefore obtain new strains expressing Ub from the URA3-marked plasmids. The *rev1*Δ strains expressing different Ub mutants were obtained similarly after having first replaced *REV1* in LHY461 by a KAN resistance cassette using homologous recombination.

To analyze the genetic interaction between *REV1* deletion and ubiquitin mutants, we spotted equivalent amounts of each strain in 5-fold serial dilutions onto yeast extract-peptone-dextrose (YPD) plates containing increasing concentrations of 4-nitroquinoline-1-oxide (4NQO, Sigma). Pictures of the plates were recorded after 3 days of growth at 30 °C.

RESULTS

NMR Structure of UBM1 and UBM2 Bound to Ubiquitin—For the determination of the solution structure of the two UBM domains, UBM1 and UBM2 of murine Pol ι in complex with ubiquitin, we expressed the two domains as GST-fusion proteins in *E. coli* and cleaved GST with thrombin. The final sequences of the domains are reported in supplemental Fig. 3. The structures of both UBMs within the UBM·ubiquitin complex are well defined, and the important features defining the UBM structures and binding mode to Ub were the same for UBM1 (Fig. 1*A*) and UBM2 (Fig. 1*B*).

The structures of the entire Ub·UBM1 and Ub·UBM2 complexes are well defined with overall backbone root mean square deviation values of 0.67 ± 14 Å and 0.54 ± 12 Å, respectively (Table 1). With the almost complete assignment of the spectra, NOE data are fully used, and a further refinement of the structures requires additional data, *e.g.* residual dipolar couplings or scalar couplings. However, averaging of these parameters over free and bound conformations has potentially much more detrimental effects on the structure than the averaging of NOEs (see also "Discussion"). Thus, we decided to stay with the given precision, which is also sufficient for the characterization of the binding interface.

The structures consisted of a yet unreported type of the helix-turn-helix motif (see "Discussion") where the first helix was longer than the second, and the turn was comprised of a highly conserved Leu-Pro motif. This motif has a similar spatial arrangement for UBM1 and UBM2 (Fig. 1*C* and supplemental Fig. 4; positioning on ubiquitin is shown in supplemental Fig. 5). In UBM1, the helices included residues 502–507 and 510–517, and in UBM2, helices included 687–692 and 695–707. These residues showed protection against exchange of amide hydrogens to deuterons in a NMR spectrum measured 30 min after buffer exchange from H_2O to D_2O, indicating the presence of hydrogen bonds.

The N termini of both UBM domains and the C terminus of UBM1 were partially folded and looped back onto the structure extending the hydrophobic surface (Fig. 1, *A* and *B*) and contributing to a small hydrophobic core. UBM1 was only comprised of a very small hydrophobic core between the

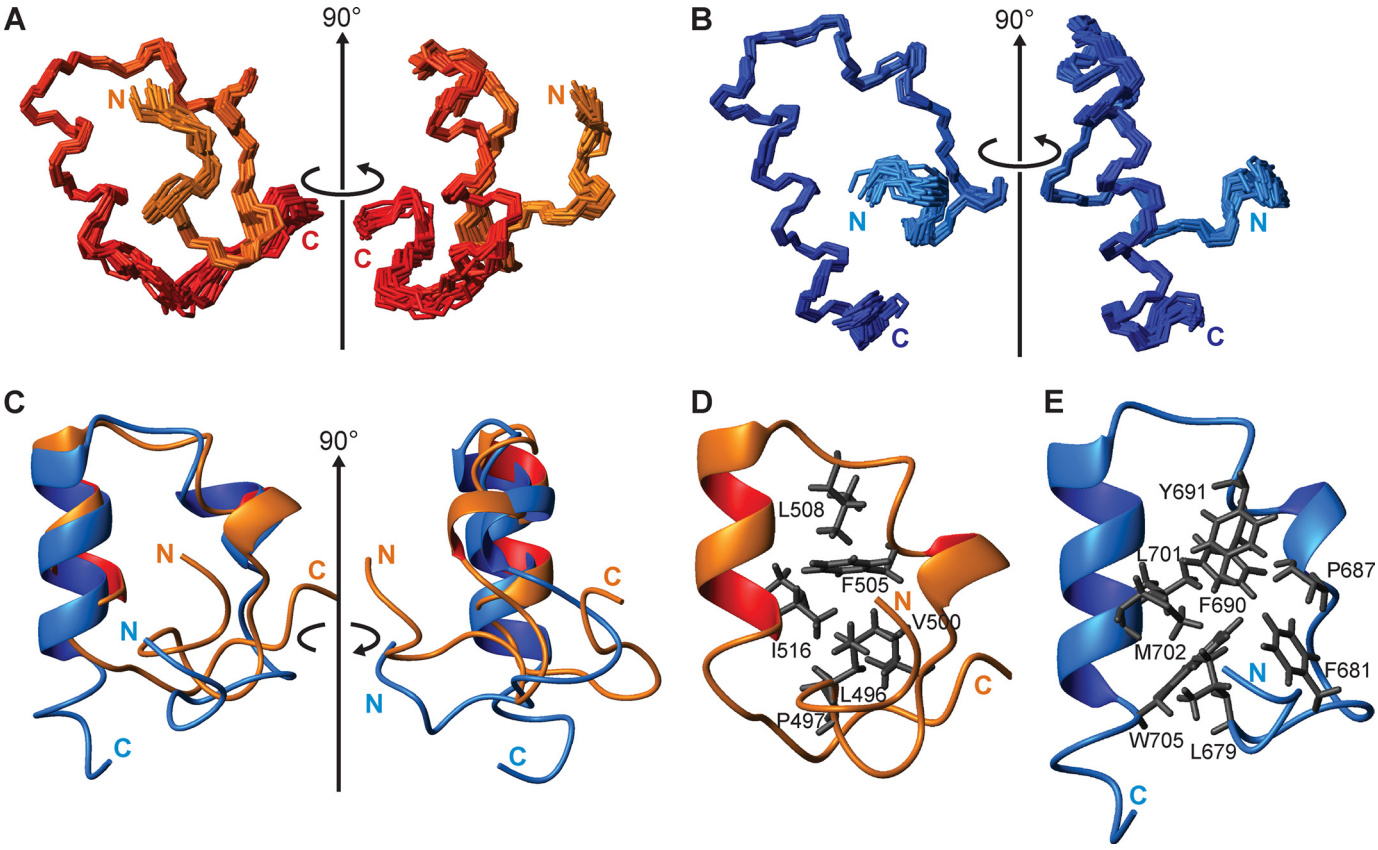

FIGURE 1. **Structural features of the UBM domains.** *A*, superposition of the 20 lowest energy NMR structures of UBM1 bound to ubiquitin (not shown), residues 491 to 526 are shown. *B*, same as *A* for UBM2; residues 675 to 710 are shown. *C*, superposition of the structures of UBM1 (*orange/red*) and UBM2 (*blue*) bound to ubiquitin (not shown). *D*, view of the hydrophobic core of UBM1; important residues are shown in *gray*. *E*, same as *D* for UBM2. Note that in all *ribbon* representations, we used the lowest energy structures that best represented the features we wanted to show in a particular figure.

two helices, which consisted of parts of the residues Leu-496, Pro-497, Val-500, Phe-505, Leu-508, and Ile-516 (Fig. 1*D*). The larger hydrophobic core of UBM2 was composed of the four aromatic side chains of Phe-681, Phe-690, Tyr-691, and Trp-705 and the aliphatic residues Leu-679, Pro-687, Leu-701, and Met-702 (Fig. 1*E*).

Our data on UBM1 and UBM2 indicate that both domains are folded in complex with ubiquitin. The generally small chemical shift changes upon titration of the free domains with ubiquitin (supplemental Fig. 6, *A* and *B*) suggest that they adopt a very similar conformation free in aqueous solution as in the complex. This conclusion is supported by heteronuclear NOE measurements between protons and nitrogens in the backbone amide groups, which provide a measure of the rigidity of the polypeptide backbone (29, 30). Although the backbone rigidity of UBM2 only marginally increased upon ubiquitin binding (Fig. 2*G*), a bigger increase in rigidity was observed with UBM1, although both leveled off at comparable values of 0.8 on the ordinate for the core of the domains. The smaller hydrophobic core of UBM1 may explain its higher structural flexibility compared with UBM2. However, thermal denaturation experiments with free UBM1 and UBM2 monitored by NMR and by CD spectroscopy failed to reveal a clear transition between the folded and unfolded state. Instead, a gradual change was observed, suggesting that the various conformations of these small domains may be in equilibrium (supplemental Fig. 7). Still, our data suggest that UBM1 and UBM2 are independently folding domains, possessing a hydrophobic core and a specific interaction surface; thus, they do not seem to change their fold upon binding to ubiquitin.

Ubiquitin-binding Surface of UBM1 and UBM2—The structural details of the binding interface between UBM1 or UBM2 and ubiquitin were delineated from intermolecular NOE interactions (Fig. 2*A*), which were part of the input for the calculation of the complex structure. For UBM1 and UBM2, 97 and 96 intermolecular UPLs, respectively, were used. Consistent with NMR titration experiments, relatively strong NOEs were observed between Leu-8 on ubiquitin and Val-500 and Val-504 on UBM1 or the corresponding positions defined by Ile-685, Val-689 on UBM2; further between Leu-508, Ile-512 (UBM1), or Leu-693, Val-697 (UBM2) and Ile-44 (Ub), as well as between Leu-508, Ile-512, and Ile-516 (UBM1) or Leu-693, Val-697, Leu-701 (UBM2), and Val-70 (Ub). In addition, for several UBM1 and UBM2 residues close to the ubiquitin C terminus, small chemical shift perturbations and weak intermolecular contacts were detectable. These results suggest that like other UBDs, UBM domains bind ubiquitin on or close to the classical patch delineated by Leu-8, Ile-44, and Val-70, which offers a mainly hydrophobic surface.

In the NMR structures of the UBM·Ub complexes, Leu-8 and Val-70 are buried within the interface, whereas Ile-44 is positioned at the edge of the binding surface (Fig. 2, *D* and *E*).

TABLE 1
Input for the structure calculation and characterization of the 20 best energy-minimized NMR structures of UBM1 or UBM2 in complex with ubiquitin

Quantity	UBM1 bound to Ub	UBM2 bound to Ub
NOE-derived UPLs[a]	2862 (UBM1, 995; Ub, 1867)	2758 (UBM2, 970; Ub, 1788)
Intraresidual ($\|i-j\|=0$)	684 (UBM1, 241; Ub, 443)	672 (UBM2, 224; Ub, 448)
Short range ($\|i-j\|=1$)	825 (UBM1, 332; Ub, 493)	760 (UBM2, 324; Ub, 436)
Medium range ($2 \le \|i-j\| \le 4$)	723 (UBM1, 297; Ub, 426)	778 (UBM2, 356; Ub, 422)
Long range ($\|i-j\| \ge 5$)	630 (UBM1, 125; Ub, 505)	548 (UBM2, 66; Ub, 482)
NOE-derived inter-UPLs	97	96
Dihedral angle constraints	432 (UBM1, 154; Ub, 278)	440 (UBM2, 164; Ub, 276)
Residual target function (Å^2)[b]	4.17 ± 0.82	8.12 ± 1.06
Residual NOE violations		
$n > 0.1$ Å	83 ± 6	92 ± 4
Maximum (Å)	0.36 ± 0.05	0.37 ± 0.07
Residual angle violations		
$n > 2.5°$	0 ± 1°	2 ± 1°
Maximum (°)	2.01 ± 1.51°	5.96 ± 1.71°
Amber energies (kcal/mol)		
Total	4537.48 ± 13.23	4549.38 ± 16.40
Van der Waals	690.23 ± 11.20	677.62 ± 15.25
Electrostatic	8574.20 ± 273.49	8476.00 ± 285.50
r.m.s.d. from ideal geometry[c]		
Bond lengths (Å)	0.00376 ± 0.00009	0.00401 ± 0.00007
Bond angles (°)	1.424 ± 0.022°	1.624 ± 0.018°
r.m.s.d. to the mean coordinates (Å)[c]		
bb (UBM domain + Ub 1–73)	0.67 ± 0.14	0.54 ± 0.12
ha (UBM domain + Ub 1–73)	0.98 ± 0.11	0.81 ± 0.11
bb (UBM domain)	0.63 ± 0.15	0.40 ± 0.10
ha (UBM domain)	1.07 ± 0.14	0.79 ± 0.11
bb (Ub 1–73)	0.32 ± 0.07	0.31 ± 0.07
ha (Ub 1–73)	0.67 ± 0.07	0.62 ± 0.08
Ramachandran plot statistics (%)[d]		
Most favored regions	68.0 ± 2.7	65.1 ± 2.6
Additionally allowed regions	28.4 ± 2.8	29.4 ± 2.4
Generously allowed regions	2.4 ± 1.1	3.2 ± 0.7
Disallowed regions	1.1 ± 0.6	2.3 ± 0.8

[a] Intramolecular UPLs between residues with sequence positions *i* and *j* are shown.
[b] The residual target function of all 40 structures calculated by CYANA is shown.
[c] r.m.s.d. indicates root mean square deviation; bb indicates backbone atoms N, C^{α}, and C′; and ha indicates all heavy atoms. UBM domain represents residues 491–526 for UBM1 and residues 675–710 for UBM2. These regions match the predicted size of the domains and are supported by long range NOEs.
[d] Ramachandran plot statistics were determined using PROCHECK (54, 55).

Compared with other UBDs, the binding surface of UBM domains is smaller and slightly shifted away from Ile-44 toward Leu-8 and Val-70. Thus, although Ile-44 clearly contributes toward the overall binding strength of UBM domains, it is not essential (see below). On the UBM side, five conserved bulky hydrophobic side chains are involved in forming the interface (Fig. 2*D*, E; methyl-methyl NOEs in supplemental Fig. 8). For UBM1, these residues are Val-500 located N-terminal of the first helix, Val-504 in the first helix, Leu-508 from the conserved Leu-Pro motif in the loop between the helices and Ile-512 and Ile-516 from the second helix. In UBM2, the respective residues are Ile-685, Val-689, Leu-693, Val-697, and Leu-701. On both domains, these side chains form a hydrophobic pocket, into which ubiquitin Val-70 and Leu-8 fit (Fig. 2, *D* and *E*).

Further characterization of the binding interface between ubiquitin and the UBMs was determined by monitoring chemical shift changes of backbone amide groups of ^{15}N-labeled UBMs upon titration with unlabeled ubiquitin (Fig. 3, *A* and *B*). The largest chemical shift changes were observed for the residues in the binding interface identified in the structure of the complex (supplemental Fig. 9). From the dependence of the chemical shift changes *versus* the concentration ratio of the two binding partners, the dissociation constant K_D toward ubiquitin can be determined. The average K_D calculated from the five residues showing the largest traceable chemical shift changes was 90 μM for UBM1 and 51 μM for UBM2, respectively (Fig. 3, *C* and *D*).

Both NMR structure calculations and NMR titration experiments suggest that Arg-42 in ubiquitin forms a salt bridge with the highly conserved acidic residues Asp-511/Glu-515 in UBM1 or Glu-700 in UBM2 (Fig. 3*E*). During energy minimization, these charged groups fulfilled in most structures (60% for UBM1 and 75% for UBM2) the distance constraints for groups forming ion pairs (31, 32). As NMR provides only indirect evidence for salt bridges, a UBM2 mutant was produced, where Glu-700 was replaced by glutamine. This conservative E700Q mutant abolishes the charge but preserves the size and shape of the side chain. To confirm the dissociation constant obtained by NMR for WT UBMs and in view of titrations with diubiquitins (see below), we decided to monitor the titrations by tryptophan fluorescence spectroscopy. However, these measurements could only be performed with UBM2, which contains a well positioned intrinsic tryptophan (Trp-705), whereas UBM1 does not contain tryptophan. Consistent with the NMR experiments, titrating increasing amounts of ubiquitin into a

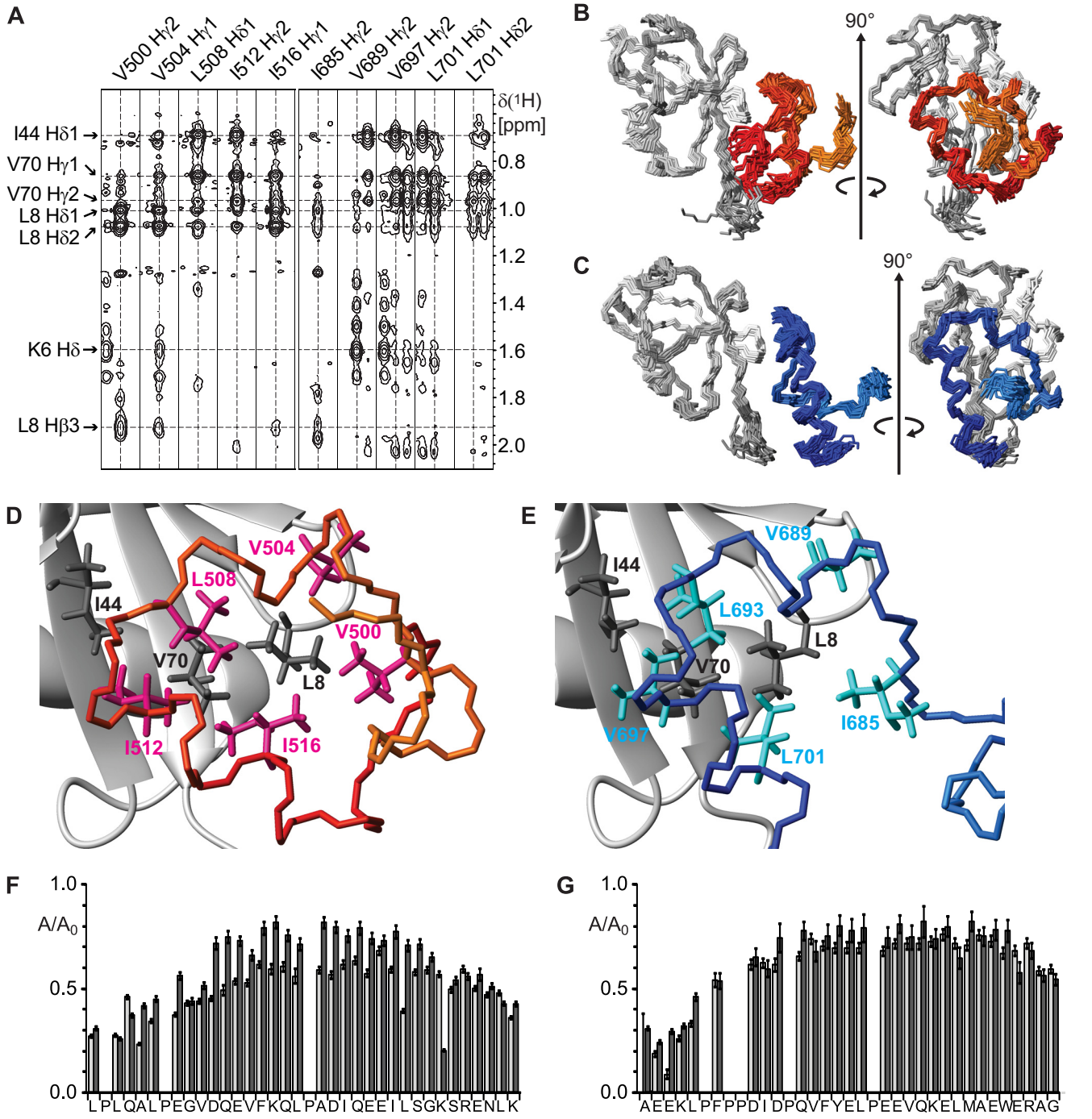

FIGURE 2. **Characterization of the binding interface between UBMs and ubiquitin.** *A*, strips extracted from a three-dimensional ^{13}C-resolved [^{1}H,^{1}H]-NOESY spectrum showing intermolecular NOEs between ubiquitin and UBM1 (*left five strips*) and between ubiquitin and UBM2 (*right*); chemical shift positions of important interface residues of ubiquitin are indicated by *arrows* on the *left*; interacting UBM residues are marked on the *top* of the individual strips. *B*, superposition of the 20 lowest energy NMR structure of the UBM1·ubiquitin complex; the root mean square deviation of the superposition is minimized for the complex (residues 491–526 of UBM1 and residues 1–73 for ubiquitin; root mean square deviation minimized only for ubiquitin see supplemental Fig. 11). *C*, superposition of the 20 lowest energy NMR structures of the UBM2·ubiquitin complex; the root mean square deviation of the superposition is minimized for the complex (residues 675–710 of UBM2 and residues 1–73 for ubiquitin). *D*, binding interface between UBM1 and ubiquitin; hydrophobic side chains involved in the interaction are shown as *stick* models, which are labeled with the residue number in *magenta* for UBM1 and in *dark gray* for ubiquitin. *E*, same as *D* for UBM2, with labeling in *cyan*. *F*, ^{15}N{^{1}H}-heteronuclear NOE values plotted *versus* the sequence of UBM1 in the absence (*light gray*) and presence (*dark gray*) of ubiquitin. *G*, same as *F* for UBM2.

solution of WT and UBM2-E700Q (Fig. 3*F*) revealed a K_D of WT UBM2 toward ubiquitin of ~50 μM (Fig. 3, *C* and *D*). Interestingly, the corresponding K_D for UBM2-E700Q was increased 3-fold to 150 μM, which confirms that the electrostatic interaction contributes substantially to the binding.

UBM Domains Bind Monoubiquitin and Lys-63- but Not Lys-48-linked Diubiquitin Chains—In response to DNA damage, PCNA can be either monoubiquitinated or Lys-63-polyubiquitinated, and the two modifications have different biological outputs. Monoubiquitination induces the fast but

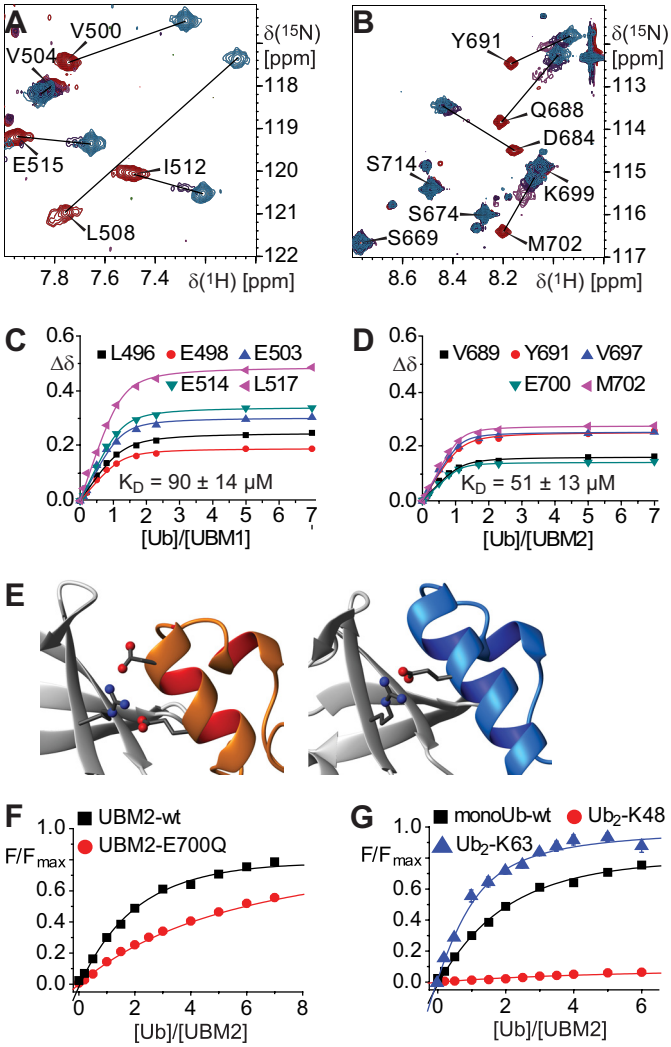

FIGURE 3. **Binding affinities derived from titration experiments.** *A*, detail of overlaid [^{1}H,^{15}N]-HSQC spectra showing chemical shift changes of backbone amide groups of ^{15}N-labeled UBM1 upon titration with unlabeled ubiquitin, the concentration ratios Ub:UBM1 are color-coded: *red*, 0.0; *magenta*, 0.5; *violet*, 1.1; and *cyan*, 5.0. *B*, same as *A* for UBM2. *C*, chemical shift changes of amide groups, Δδ, *versus* the concentration ratio UBM1:Ub for selected residues in UBM1. An average dissociation constant, K_D, of 90 μM was obtained from the curves. *D*, same as *C* but for UBM2; K_D = 51 μM. *E*, electrostatic interaction between UBM1 (*left*) or UBM2 (*right*) and ubiquitin. The involved residues are Asp-511/Glu-515 in UBM1, Glu-700 in UBM2 and Arg-42 in ubiquitin (also see supplemental Fig. 12). *F*, titrations of UBM2 with ubiquitin monitored by fluorescence spectroscopy; the UBM2 mutant E700Q, which abolishes the electrostatic interaction, is compared with UBM2-WT. *G*, titrations of UBM2 with ubiquitin, Lys-48-diubiquitin, or Lys-63-diubiquitin monitored by fluorescence spectroscopy. The *abscissa* depicts the molar ratio between ubiquitin and UBM2, *i.e.* one diubiquitin corresponds to two Ub.

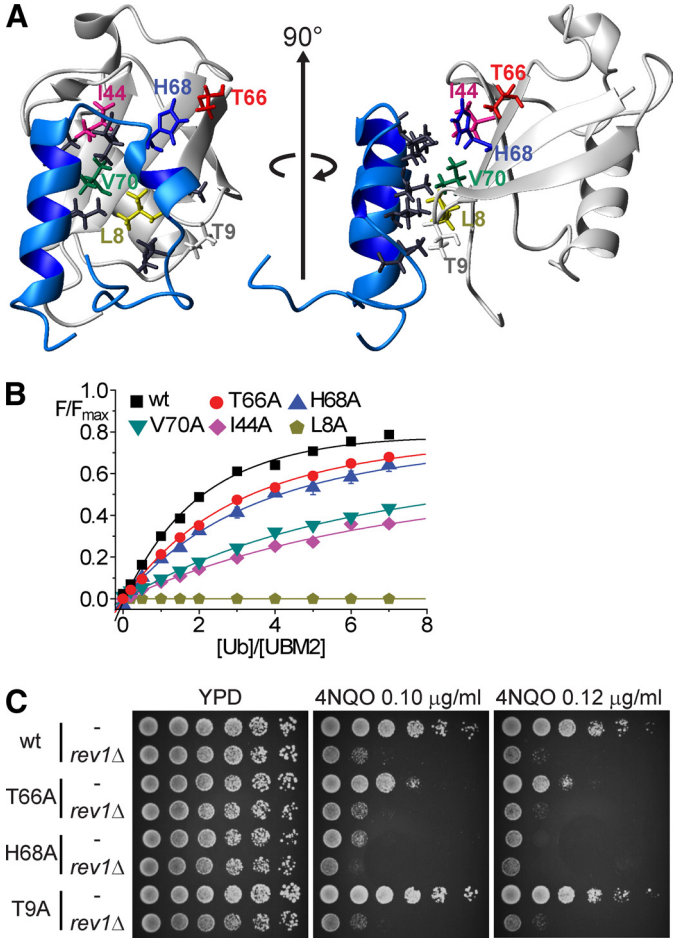

FIGURE 4. ***In vitro* and *in vivo* mutational analyses.** *A*, *ribbon* representation of the complex of ubiquitin (*gray*) and UBM2 (*blue*) showing the positions of the mutated amino acids (*stick plot*) used to characterize the interface between Ub and UBM2; the indicated residues were individually mutated to Ala. *B*, concentration ratio of Ub:UBM2 *versus* the fluorescence signal obtained upon titration of UBM2 with Ub-WT and the Ub mutations indicated in the figure; the same color code is used for the residues as in *A*. *C*, assay of the interaction between UBMs and Ub in different *S. cerevisiae* strains; for WT ubiquitin and the ubiquitin mutants T66A, H68A, and T9A, a strain with or without *REV1* (*rev1*Δ) was constructed. Sensitivity of all eight strains on yeast extract-peptone-dextrose (YPD) medium subjected to increasing concentrations of 4NQO was monitored; growth of the same strains on YPD only is shown as a control.

error-prone translesion synthesis (33), whereas Lys-63-polyubiquitinated PCNA induces a slower and less error-prone repair pathway using sister strand recombination (34, 35). This fact raises the question of whether UBM domains show a differential binding affinity and/or specificity toward monoubiquitin and ubiquitin chains. We measured the binding affinities of UBM2 to Lys-48-linked diubiquitin and to Lys-63-linked diubiquitin using fluorescence spectroscopy. UBM2 was unable to bind to Lys-48-linked diubiquitin (Fig. 3*G*), which is not surprising as the UBM binding site is occluded in Lys-48-linked chains (10). In contrast, Lys-63-linked diubiquitin were readily bound by UBM2 with an apparently decreased K_D of 14 μM compared with monoubiquitin. The additive increase in binding of UBM2 to Lys-63-linked diubiquitin chains may be due to the fact that both UBM binding sites are accessible in Lys-63-linked diubiquitin. Thus, UBMs do not seem to be specific Lys-63-linked chain-binding domains but bind any accessible ubiquitin interface in monoubiquitin or ubiquitin chains.

Mutational Analysis of Hydrophobic UBM·Ubiquitin Binding Surface—Based on the NMR structure of the UBM·Ub complex, we investigated the interaction between UBM2 and several ubiquitin mutants (L8A, I44A, T66A, H68A, and V70A) using titration experiments monitored by tryptophan fluorescence spectroscopy. The localization of the mutated residues on the ubiquitin surface is displayed in Fig. 4*A*. For the L8A Ub mutant, no binding to UBM2 could be detected (Fig. 4*B*). The other Ub mutants showed increased K_D values

of ~85 μM (1.7-fold increase), 105 μM (2.1-fold increase), 245 μM (4.9-fold increase), and 330 μM (6.6-fold increase) for T66A, H68A, V70A, and I44A respectively (Fig. 4*B*). Although T66A and H68A are not directly at the interface, their K_D values were slightly increased. This assay also confirms that the I44A Ub mutant is still able to interact with UBM2, albeit weakly (16). In summary, our quantitative binding experiments combined with the mutational analysis confirm the functional importance of the hydrophobic surface residues involved in UBM binding and indicate that UBM domains interact with ubiquitin on a surface that is similar to other ubiquitin-binding proteins but slightly shifted away from Ile-44 toward Leu-8 and Val-70.

A Functional Ubiquitin-UBM Interaction Is Required for Polymerase ι Function in Vivo—The UBM-ubiquitin interaction is essential for Pol ι and Rev1 function in *Saccharomyces cerevisiae* and mammalian cells (16, 36, 37). This finding is based on experiments with either UBM deletions or UBM mutants, where the conserved Leu-Pro motif in the loop was altered, likely disrupting the entire fold (16). To specifically study the functional importance of the interaction between the UBMs of Y-family polymerases and ubiquitin, we used unmodified UBM domains and specific mutants of ubiquitin. For this assay, we used yeast strains in which the four endogenous Ub genes had been deleted and replaced by a plasmid encoding wild type or mutated Ub (4). In *S. cerevisiae*, Rev1 is the sole Y-family DNA polymerase carrying UBM domains. Like mammalian Pol ι, Rev1 has two predicted UBM domains in its C terminus, but only the second one (UBM2) is required for Rev1 function *in vivo* (36).

Unfortunately L8A, V70A, or I44A Ub mutants could not be analyzed as strains harboring these mutations are not viable (4). However, strains individually expressing the H68A, T66A, and T9A Ub mutants are viable and were used for the study. H68A and T66A mutants weaken the interaction with mouse UBM2 (Fig. 4*B*), whereas based on our structure of the UBM·Ub complex, the T9A mutant should not affect the binding. Each Ub mutant was analyzed in strains bearing either wild type or a *REV1* deletion. We assessed the sensitivity of these strains to increasing amounts of the DNA-alkylating agent 4NQO (Fig. 4*C*). 4NQO allows for assessment of Rev1 function more specifically than other DNA-damaging agents because the only other UBD containing Y-family polymerase in yeast (Rad30) is not involved in 4NQO resistance (38). As expected, *rev1*Δ cells expressing wild type Ub were very sensitive to 4NQO. Furthermore, *REV1* cells expressing Ub-T66A were sensitive to 4NQO but to a lesser extent. This phenotype is consistent with a partial loss of the interaction between UBM2 of Rev1 and Ub. Importantly, *rev1*Δ cells expressing Ub-T66A were as sensitive to 4NQO as *rev1*Δ cells expressing wild type Ub, indicating that the 4NQO sensitivity results from an impaired Rev1 function. *REV1* cells expressing the Ub-H68A mutant were also sensitive to 4NQO, but this sensitivity was further enhanced after deletion of *REV1*, indicating that the H68A mutation in Ub impairs not only Rev1 function but also other processes. Finally, *REV1* and *rev1*Δ strains expressing the Ub-T9A mutant displayed the same sensitivity to 4NQO as the corresponding strains expressing wild type Ub. This indicates that Thr-9 of Ub is not required for Rev1 function *in vivo*. Taken together, these results demonstrate that the specific interaction of ubiquitin with the UBM domains of Rev1 is required to regulate TLS polymerases at sites of DNA damage *in vivo*.

DISCUSSION

We report the NMR solution structures of ubiquitin in complex with two UBM domains, UBM1 and UBM2, from murine Pol ι, which is involved in translesion synthesis in eukaryotic cells. The interaction between UBMs and ubiquitin is weak, which results in averaged NMR spectra of the free and bound form of the UBMs, *i.e.* using a 1:1 ratio for the two partners in the complex may not produce an NMR spectrum with the signals in the position of the complex. Furthermore, depending on the dynamic properties the NMR signal may broaden and become undetectable. Fig. 3, *A* and *B*, show that the NMR signals reach their final position only with ~4-fold overtitration of ubiquitin and that some signals during the titration from the free to the overtitrated position are missing. For a more precise characterization of the bound state of the NMR-observable, isotope-labeled partner, we used overtitration of the binding partner, which is not visible (unlabeled) in the NMR spectrum (see "Experimental Procedures" for details).

UBM1 and UBM2 have a well defined structure; they fold independently of their binding partner ubiquitin with a hydrophobic core and can therefore be classified as true domains. Both UBMs consist of a well conserved helix-turn-helix motif and adjacent folded stretches on both sides with an overall domain size of ~35 residues and constitute a new kind of fold (18). The only known domain structurally similar to UBM2 is the C-terminal subdomain of headpiece in villin/advillin, as determined using DaliLite (version 3) (39). The 36-residue subdomain consisting of three helices has been reported to fold independently and includes a helix-turn-helix motif, with a similar Leu-Pro turn between helices 2 and 3 (40); helix 1 is in a similar spatial position as the N terminus of UBM2. DaliLite failed to find a match for UBM1, but it still overlaps with the small villin/advillin subdomain. The UBM1 and UBM2 domains free in solution appear to neither fold cooperatively nor unfold at a specific temperature (supplemental Fig. 7). This behavior is likely due to their small size with a very limited hydrophobic core and the low content of secondary structure. Thus, under physiological conditions, several partially unfolded conformations may be present.

The UBMs bind ubiquitin on the classical binding patch delineated by Leu-8, Ile-44, and Val-70 shifted toward Leu-8 and Val-70. The interface structure shows that both Leu-8 and Val-70 perfectly fit into a hydrophobic pocket formed by the conserved bulky side chains from either of the two UBMs (Fig. 2, *D* and *E*). This is supported by the binding data (Fig. 4*B*), which show that Leu-8 is the most important residue. Whereas the L8A mutant abolishes binding, this is not the case for Val-70, which may be due to the smaller size difference upon mutation to alanine. Ile-44 is not part of this pocket and is instead located at the edge of the hydrophobic

surface of the UBMs. This could explain why Ile-44 was not originally thought to be important for binding (16).

Electrostatic interactions between the charged end groups of different amino acids are proposed to contribute to ubiquitin binding in several UBDs (*e.g.* UBA, UIM, CUE (11, 41, 42)). For UBM1 and UBM2, we show that a salt bridge between Arg-42 of Ub and conserved glutamate residues in UBMs contributes to the binding because the binding affinity decreases by a factor of three when glutamate is replaced with glutamine. This observation explains the conservation of the acidic residues in the different UBMs (supplemental Fig. 10). Arg-42 appears to also be involved in ion pairing for the interaction of ubiquitin with other UBDs (11, 41, 42). Based on this biophysical data and the observation that the R42A substitution is lethal in yeast (4), one could speculate that Arg-42 is involved in the interaction between various UBDs and Ub. Although we cannot exclude that the observed lethality could simply be a result of the large size difference of the side chains, we speculate that salt bridges might be more abundant in ubiquitin binding than currently appreciated. NMR data only yield indirect evidence for the presence of a salt bridge such as changes in chemical shifts or line width. Thus, in general, evidence for salt bridges only emerges during energy refinement of NMR structures if neighboring charges happen to be close enough to interact. Therefore, it is not surprising that electrostatic interactions have not been emphasized in ubiquitin binding so far. However, the fact that the small UBMs utilize salt bridges to stabilize the interaction as well as the fact that these small domains rely on Leu-8 and Val-70 for ubiquitin binding may indicate that the ubiquitin binding surface is more diverse than originally described (2, 14, 43).

The response of the cell to DNA damage is associated with Lys-63-linked ubiquitin chains (14). Our data suggest that UBMs are able to bind any ubiquitin moiety, in a chain or not, as long as the binding surface is free. The increased binding toward Lys-63-linked diubiquitin appears to be mediated by normal cooperativity due to the presence of a second binding site and not due to any specific effect of the Lys-63-linked Ub chain. This behavior is reminiscent of the interaction mode, termed allovalency, between multisite phosphorylated substrates and their receptors. We speculate that this mechanism might be underlying most Lys-63-linked chain-specific binding events. The inability of the UBMs to bind Lys-48-linked diubiquitin is likely due to the binding site being occluded by the chain conformation.

The integrity of the UBM fold is functionally important (16), and we therefore characterized cell survival upon DNA damage using ubiquitin surface mutants. Interestingly, we found that cells expressing Ub-T66A are sensitive to 4NQO and that this phenotype can be attributed to an impaired function of Rev1. This result confirms our *in vitro* data indicating that UBMs exhibit weaker affinity for this Ub mutant. Furthermore, as subtle changes in the affinity of UBMs for Ub seriously impair the function of Rev1 *in vivo*, this suggests that the function of Rev1 is directly linked to the binding strength of its UBM to Ub. Previous publications indicate that the UBDs of TLS polymerases function to recruit the polymerases to stalled replication forks (44, 45). Similar to processive polymerases, TLS polymerases interact with PCNA irrespectively of its ubiquitination status via their PCNA interaction peptides (45, 46). The affinities of the PCNA interaction peptides of human Pol ι and Pol η for PCNA have recently been shown to be ~0.4 μM (47). This is >100 times stronger than the binding of Ub to the UBMs of mouse Pol ι (~90 μM for UBM1 and 50 μM for UBM2) or to the UBZ of human Pol η (~80 μM) (48). Therefore, it appears unlikely that the recruitment of TLS polymerases to replication foci depends on a specific interaction of its UBM domains with monoubiquitinated PCNA. It thus remains unclear how the low affinity interaction between UBDs and Ub governs the recruitment and function of TLS polymerases at stalled replication forks. An intriguing speculation is that it occurs via a similar mechanism proposed for multisite phosphorylation interactions. However, in TLS polymerases, the allovalency would occur between the UBM domains within their long unstructured C termini and ubiquitinated members of the replication foci. In this case, the correct localization of the TLS polymerases would depend primarily on the amount of ubiquitin present within the foci and would therefore be highly dynamic. Removal of ubiquitin moieties within the range of the unstructured C terminus of TLS polymerases could then enable the switch between polymerases at stalled replication forks. This model would also account for why the rather small decrease in the affinity between ubiquitin and yeast UBM could have such a drastic effect on cell survival upon 4NQO treatment.

As previously mentioned, the UBMs of Pol ι bind ubiquitin on the classical hydrophobic patch by interacting with the same side chains, mainly Leu-8, Ile-44, and Val-70, as do other α-helical UBDs. Because the UBMs represent a novel helix-turn-helix fold, the orientation of the helices on ubiquitin differs from other α-helical UBDs, which have distinct binding modes, *e.g.* Refs. 49–52. The UBMs are very small domains with a binding surface that is smaller than other UBDs. Consequently, Ile-44 is not entirely buried in the interface, and His-68 interacts with the UBMs only weakly.

Our structure of the ubiquitin·UBM2 complex is very similar to the central portion of the recently published structure of the GB1-fusion of UBM2 of human Pol ι (supplemental Table 2) (18). The N-terminal part exhibits a different fold in which it is folded back on the domain. This difference is probably a consequence of the different amino acid sequence with murine UBM2 containing PFPP (with penultimate proline in the *cis* conformation) and human UBM2 containing only one proline in this region. The murine structures of the weakly binding protein·protein complex seem to be less precise than the human homologs. However, we did not use residual dipolar couplings as structural restraints because the presence of fast-exchanging conformations of the UBM domains produces averaged residual dipolar coupling values, which may easily result in an artificial precision of the structural bundle.

The binding of ubiquitin to human UBM2 (18) is about three times stronger than for murine UBM2. We determined binding affinities with NMR and fluorescence spectroscopy, whereas for human UBM2, isothermal titration calorimetry was used. The observed difference could be inherent or may be in part due the use of a fusion protein in which human

UBM2 accounts for less than one-third of the construct. Interestingly, the K_D value measured for the similarly sized UBZ domain of Pol η (48) was comparable with the ones we obtained for murine UBM2.

In general, UBM domains are not widespread within the proteome of human and yeast. In humans, the proteins possessing these domains are Rev1, Pol ι, XPG, and MULE, whereas in yeast, three proteins possess UBM domains; Rev1, Rad2 (the homolog of the human XPG protein), and the HECT E3 ligase Tom1 (the homolog of MULE) (53). With the exception of Tom1, all proteins are involved in DNA damage processing. The role of Tom1 is reported to be mRNA export, transcriptional activation, and degradation of histones. Therefore, the cells might limit the use of UBM domains to DNA proximal processes.

Acknowledgments—We thank Dr. K. Hoffmann for the bioinformatic analysis, C. Rupp and C. Brasseur for technical assistance, Dr. L. Hicke for providing the basic yeast strain, and Dr. T. Roberts for critical reading of the manuscript.

REFERENCES

1. Komander, D., Clague, M. J., and Urbé, S. (2009) *Nat. Rev. Mol. Cell Biol.* **10,** 550–563
2. Hicke, L., Schubert, H. L., and Hill, C. P. (2005) *Nat. Rev. Mol. Cell Biol.* **6,** 610–621
3. Hurley, J. H., Lee, S., and Prag, G. (2006) *Biochem. J.* **399,** 361–372
4. Sloper-Mould, K. E., Jemc, J. C., Pickart, C. M., and Hicke, L. (2001) *J. Biol. Chem.* **276,** 30483–30489
5. Ikeda, F., and Dikic, I. (2008) *EMBO Rep.* **9,** 536–542
6. Raasi, S., and Pickart, C. M. (2003) *J. Biol. Chem.* **278,** 8951–8959
7. Varadan, R., Assfalg, M., Raasi, S., Pickart, C., and Fushman, D. (2005) *Mol. Cell* **18,** 687–698
8. Sato, Y., Yoshikawa, A., Yamashita, M., Yamagata, A., and Fukai, S. (2009) *EMBO J.* **28,** 3903–3909
9. Varadan, R., Assfalg, M., Haririnia, A., Raasi, S., Pickart, C., and Fushman, D. (2004) *J. Biol. Chem.* **279,** 7055–7063
10. Varadan, R., Walker, O., Pickart, C., and Fushman, D. (2002) *J. Mol. Biol.* **324,** 637–647
11. Long, J., Gallagher, T. R., Cavey, J. R., Sheppard, P. W., Ralston, S. H., Layfield, R., and Searle, M. S. (2008) *J. Biol. Chem.* **283,** 5427–5440
12. Lowe, E. D., Hasan, N., Trempe, J. F., Fonso, L., Noble, M. E., Endicott, J. A., Johnson, L. N., and Brown, N. R. (2006) *Acta Crystallogr. Sect. D Biol. Crystallogr.* **62,** 177–188
13. Raasi, S., Varadan, R., Fushman, D., and Pickart, C. M. (2005) *Nat. Struct. Mol. Biol.* **12,** 708–714
14. Pickart, C. M., and Fushman, D. (2004) *Curr. Opin. Chem. Biol.* **8,** 610–616
15. Waters, L. S., Minesinger, B. K., Wiltrout, M. E., D'Souza, S., Woodruff, R. V., and Walker, G. C. (2009) *Microbiol. Mol. Biol. Rev.* **73,** 134–154
16. Bienko, M., Green, C. M., Crosetto, N., Rudolf, F., Zapart, G., Coull, B., Kannouche, P., Wider, G., Peter, M., Lehmann, A. R., Hofmann, K., and Dikic, I. (2005) *Science* **310,** 1821–1824
17. Zhou, P., Lugovskoy, A. A., and Wagner, G. (2001) *J. Biomol. NMR* **20,** 11–14
18. Bomar, M. G., D'Souza, S., Bienko, M., Dikic, I., Walker, G. C., and Zhou, P. (2010) *Mol. Cell* **37,** 408–417
19. Schumann, F. H., Riepl, H., Maurer, T., Gronwald, W., Neidig, K. P., and Kalbitzer, H. R. (2007) *J. Biomol. NMR* **39,** 275–289
20. Fielding, L. (2007) *Prog. Nucl. Magn. Reson. Spectrosc.* **51,** 219–242
21. Zwahlen, C., Legault, P., Vincent, S. J., Greenblatt, J., Konrat, R., and Kay, L. E. (1997) *J. Am. Chem. Soc.* **119,** 6711–6721
22. Herrmann, T., Güntert, P., and Wüthrich, K. (2002) *J. Biomol. NMR* **24,** 171–189
23. Herrmann, T., Güntert, P., and Wüthrich, K. (2002) *J. Mol. Biol.* **319,** 209–227
24. Güntert, P., Mumenthaler, C., and Wüthrich, K. (1997) *J. Mol. Biol.* **273,** 283–298
25. Case, D. A., Darden, T. A., Cheatham, I. T. E., Simmerling, C. L., Wang, J., Duke, R. E., Luo, R., Merz, K. M., Pearlman, D. A., Crowley, M., Walker, R. C., Zhang, W., Wang, B., Hayik, S., Roitberg, A., Seabra, G., Wong, K. F., Paesani, F., Wu, X., Brozell, S., Tsui, V., Gohlke, H., Yang, L., Tan, C., Mongan, J., Hornak, V., Cui, G., Beroza, P., Mathews, D. H., Schafmeister, C., Ross, W. S., and Kollman, P. A. (2006) AMBER9 (University of California, San Francisco)
26. Wang, J. M., Cieplak, P., and Kollman, P. A. (2000) *J. Comput. Chem.* **21,** 1049–1074
27. Koradi, R., Billeter, M., and Wüthrich, K. (1996) *J. Mol. Graph* **14,** 51–55
28. Groemping, Y., and Hellmann, N. (2005) *Curr. Protoc. Protein Sci.* **39,** 20.28.21–20.28.27
29. Renner, C., Schleicher, M., Moroder, L., and Holak, T. A. (2002) *J. Biomol. NMR* **23,** 23–33
30. Zhu, G., Xia, Y., Nicholson, L. K., and Sze, K. H. (2000) *J. Magn. Reson.* **143,** 423–426
31. Barlow, D. J., and Thornton, J. M. (1983) *J. Mol. Biol.* **168,** 867–885
32. Musafia, B., Buchner, V., and Arad, D. (1995) *J. Mol. Biol.* **254,** 761–770
33. Stelter, P., and Ulrich, H. D. (2003) *Nature* **425,** 188–191
34. Chiu, R. K., Brun, J., Ramaekers, C., Theys, J., Weng, L., Lambin, P., Gray, D. A., and Wouters, B. G. (2006) *PLoS. Genet.* **2,** 1070–1083
35. Zhang, H., and Lawrence, C. W. (2005) *Proc. Natl. Acad. Sci. U.S.A.* **102,** 15954–15959
36. Guo, C., Tang, T. S., Bienko, M., Parker, J. L., Bielen, A. B., Sonoda, E., Takeda, S., Ulrich, H. D., Dikic, I., and Friedberg, E. C. (2006) *Mol. Cell. Biol.* **26,** 8892–8900
37. Wood, A., Garg, P., and Burgers, P. M. (2007) *J. Biol. Chem.* **282,** 20256–20263
38. Sabouri, N., Viberg, J., Goyal, D. K., Johansson, E., and Chabes, A. (2008) *Nucleic Acids Res.* **36,** 5660–5667
39. Holm, L., Kääriäinen, S., Rosenström, P., and Schenkel, A. (2008) *Bioinformatics* **24,** 2780–2781
40. Vermeulen, W., Vanhaesebrouck, P., Van Troys, M., Verschueren, M., Fant, F., Goethals, M., Ampe, C., Martins, J. C., and Borremans, F. A. (2004) *Protein Sci.* **13,** 1276–1287
41. Hirano, S., Kawasaki, M., Ura, H., Kato, R., Raiborg, C., Stenmark, H., and Wakatsuki, S. (2006) *Nat. Struct. Mol. Biol.* **13,** 272–277
42. Prag, G., Misra, S., Jones, E. A., Ghirlando, R., Davies, B. A., Horazdovsky, B. F., and Hurley, J. H. (2003) *Cell* **113,** 609–620
43. Yin, L. M., Russell, N. S., Cheng, D. M., Peng, J. M., and Wilkinson, K. D. (2006) *Isr. J. Chem.* **46,** 159–169
44. Lehmann, A. R. (2006) *DNA Repair* **5,** 404–407
45. Guo, C., Kosarek-Stancel, J. N., Tang, T. S., and Friedberg, E. C. (2009) *Cell Mol. Life Sci.* **66,** 2363–2381
46. Vidal, A. E., Kannouche, P., Podust, V. N., Yang, W., Lehmann, A. R., and Woodgate, R. (2004) *J. Biol. Chem.* **279,** 48360–48368
47. Hishiki, A., Hashimoto, H., Hanafusa, T., Kamei, K., Ohashi, E., Shimizu, T., Ohmori, H., and Sato, M. (2009) *J. Biol. Chem.* **284,** 10552–10560
48. Bomar, M. G., Pai, M. T., Tzeng, S. R., Li, S. S., and Zhou, P. (2007) *EMBO Rep.* **8,** 247–251
49. Lee, S., Tsai, Y. C., Mattera, R., Smith, W. J., Kostelansky, M. S., Weissman, A. M., Bonifacino, J. S., and Hurley, J. H. (2006) *Nat. Struct. Mol. Biol.* **13,** 264–271
50. Ohno, A., Jee, J., Fujiwara, K., Tenno, T., Goda, N., Tochio, H., Kobayashi, H., Hiroaki, H., and Shirakawa, M. (2005) *Structure* **13,** 521–532
51. Prag, G., Lee, S., Mattera, R., Arighi, C. N., Beach, B. M., Bonifacino, J. S., and Hurley, J. H. (2005) *Proc. Natl. Acad. Sci. U.S.A.* **102,** 2334–2339
52. Wang, Q., Young, P., and Walters, K. J. (2005) *J. Mol. Biol.* **348,** 727–739
53. Hofmann, K. (2009) *DNA Repair* **8,** 544–556
54. Laskowski, R. A., Macarthur, M. W., Moss, D. S., and Thornton, J. M. (1993) *J. Appl. Crystallogr.* **26,** 283–291
55. Morris, A. L., MacArthur, M. W., Hutchinson, E. G., and Thornton, J. M. (1992) *Proteins Struct. Funct. Genet.* **12,** 345–364